Iranian Journal of Catalysis 10(2), 2020, 111-117

IRANIAN JOURNAL OF CATALYSIS

Effect of acidity and physical properties of nanozeolite catalyst on hydrocracking of vacuum gas oil

Mina Hadi[a], Hamid Reza Bozorgzadeh[a,*], Hamid Reza Aghabozorg[a], Mohammad Reza Ghasemi[b]

[a]*Catalysis Research Division, Research Institute of Petroleum Industry (RIPI), Tehran, Iran.*

[b]*Faculty of Engineering and Technology, Tehran North Branch, Islamic Azad University, Tehran, Iran.*

Received 16 April 2019; received in revised form 20 August 2019; accepted 1 September 2019

ABSTRACT

In this study, beta nanozeolite, ultra-stable Y zeolite (USY) and amorphous silica-alumina (ASA) were synthesized. These compounds were used as the support of hydrocracking catalyst. Ni-Mo/beta zeolite-ASA and Ni-Mo/USY zeolite-ASA catalysts were prepared by the impregnation method. The samples were characterized with X-Ray diffraction (XRD), field emission-scanning electron microscopy (FE-SEM), temperature programmed desorption (TPD) and BET methods. Catalytic behavior of these catalysts was evaluated on hydrocracking of vacuum gas oil at 400 ℃ and 55 bar in a fixed bed continuous microreactor. The XRD patterns of the prepared samples determined the phase structure of the samples. FE-SEM images of the nanozeolites indicated that the particle sizes of them are less than 10 nm. The results indicated that the catalyst containing USY with higher pore diameter and acidity was more useful in middle distillate products (87%), while the conversion of the catalyst containing beta zeolite was more than the other catalysts (44.8%).

***Keywords**: Beta nanozeolite, USY nanozeolite, Acidity, Hydrocracking, Middle distillate.*

1. Introduction

Hydrocracking is a petrochemical process that converts petroleum fractions with high-boiling point, into more useful products such as middle distillate in the presence of H_2 and catalysts [1]. Generally, hydrocracking catalysts are composed of acidic supports (such as alumina, zeolites, amorphous silica-alumina) and active metals e.g. (Mo, W) with promoters e.g. (Ni, Co) [2]. The catalytic properties of zeolites are mainly related to their acidic properties [3,4]. Meanwhile, nanozeolites have some superior physicochemical properties and high H-transfer ability [5]. USY zeolite is widely used as the active component in the petrochemical process, because of its relatively high acid strength, controlled density of acid sites, and high hydrogen transfer ability [6,7]. Beta zeolite has a high Si/Al ratio and exhibits higher catalytic activity, lower hydrogen transfer capacity, and lower catalyst deactivation by self-poisoning [8]. Amorphous silica-alumina (ASA) is the acidic support in many commercial catalysts.

*Corresponding author.
E-mail address: bozorgzadehhr@ripi.ir (H.R. Bozorgzadeh)

Besides, in this compound, the activity is attributed to both Lewis- and Bronsted-type acid sites which are distributed over the catalyst surface [9]. Generally, decreasing the particle size of the zeolites leads to higher external surface areas and more exposed active sites, which have an effect on the performance of the nanozeolites [10]. In addition, the catalyst containing nanozeolite produced fewer light and more middle distillates products. In other words, diffusion of the molecules is strongly favored in the very small crystallines of the nanozeolites, and the secondary cracking of the intermediate product molecules is reduced [11].

Dik et al. [1] studied the hydrocracking of vacuum gas oil over Ni-Mo/zeolite-Al_2O_3 catalysts. They proved that the catalyst having beta zeolite with the smallest average particle size had the highest hydrocracking activity. However, the catalyst containing Y zeolite was more appropriate in middle distillates and is attributed to optimal zeolite acidity and desired availability of the acid sites for bulky molecules of the heavy feedstock. Recently, Heuchel and co-workers [12] studied the influence of porosity and active sites of zeolites Y and

beta on the co-cracking of n-decane. They found that the activity of the catalysts depends on the number of Bronsted acid sites; zeolites with a low acid site concentration showed lower and more stable conversion. Even though role of zeolite in composite catalyst for hydrocracking is well-known, effect of zeolite structure and properties on hydrocracking activity is not discussed in previous work. In this work, the effect of zeolite physical properties and the strength of acid sites on hydrocracking activity was investigated. Thus, beta nanozeolite, ASA and USY nanozeolite were prepared. Using these compounds as supports, Ni-Mo catalysts were made by the impregnation method. These catalysts were characterized by conventional methods. Also, hydrocracking of vacuum gas oil at 400 ℃ and 55 bar evaluated the catalytic performance of the samples.

2. Experimental

2.1. Materials

Tetraethylammonium hydroxide (TEAOH) (Aldrich, 20% by weight solution), Ludox colloidal silica (Aldrich, 40% suspension in water) and aluminum isopropylate (Sigma, 99%), were used for the synthesis of beta nanozeolite. Na-Y zeolite was purchased from RIPI (Research Institute of Petroleum Industry), ammonium nitrate (Merck, 99%), ammonium acetate (Merck, 99%) and ammonium fluorosilicate (Merck, 99%) were used for Y zeolite modification. Aluminum sulfate hexadecahydrate (Fluka, 99%), aluminum hydroxide (Merck, 99%) and sodium silicate (commercial, 19%SiO_2) were used for the synthesis of silica-alumina. The catalyst was prepared with ammonium heptamolybdate (Merck, 99%) and nickel nitrate (Merck, 99%).

2.2. Preparation of support

Beta nanozeolite was prepared using aluminum isopropylate as a source of aluminum and silica sol in aqueous tetraethylammonium hydroxide. The molar composition of the gel prepared at room temperature was as below:

25 SiO_2: 0.25 Al_2O_3: 9 TEAOH: 295 H_2O

The sample was exposed to hydrothermal treatment of the nucleated gel carried out in a teflon lined stainless steel autoclave, in a static condition at 140 ℃ for 6 days. The obtained crystalline materials were purified in three steps consisting of high-speed centrifugation at 6000 rpm for 30 min, removal of the mother liquor, and dispersion in deionized water. The resulting solid product was separated by centrifugation and washed with deionized water until achieving pH<9. The wet solids were dried at 110 °C for 4 h and calcined at 550 ℃ for 4 h in the presence of air.

Amorphous silica-alumina (ASA) was prepared using the method of sequential precipitation according to the technique described in the previous studies [13]. Initially, aluminum hydroxide was precipitated by mixing aluminum sulfate solution and aqueous ammonia solution at 60 °C in pH=8.0 under intensive stirring. Aqueous solution of sodium silicate was added to the obtained suspension at the same temperature. The product was recovered by filtration and washed with water until SO_4^{2-} was not detected in filtrate. The prepared filter cake was spray-dried by using a Buchi 190. The obtained powder after heating at 120 ℃ for 4 h, was calcined in air at 700 °C for 4 h in air.

For preparation of NH_4Y, Y zeolite was ion-exchanged with 1.0 M NH_4NO_3 aqueous solution 3 times at 80 ℃ for 2 h. The modified Y zeolites were separated by filtration, washed with deionized water and dried in an oven at 110 ℃ for 4 h [4]. For preparation of USY zeolite in a flask, NH_4Y and 1.0 M ammonium acetate solution at 75 ℃, after that, the $(NH_4)_2$ SiF_6 solution were added in dropwise to the flask. The mixture was stirred at 95 ℃ for 24 h, thoroughly washed with boiling water, and then dried at 110 ℃ overnight and calcined at 550 ℃ for 4 h in the presence of air [8].

Amorphous silica-alumina (60 wt. %), desired nanozeolites (20 wt. %) and a binder (partially acid-peptized alumina, SASOL, SB-1) were mixed to prepare a support for hydrocracking catalyst. The obtained paste was extruded and left at room temperature for a few hours. The extruded sample was placed in an oven at 110 ℃ for 4 h. The dried sample was finally calcined at 550 ℃ for 4 h.

2.3. Preparation of catalyst

The Ni-Mo catalysts were prepared by the incipient wetness impregnation method using a rotary evaporator. An appropriate amount of ammonium heptamolybdate and nickel nitrate was used in the aqueous solution. The amount of added water was calculated from the total pore volume of the support. The catalyst was dried in the rotary vacuum evaporator for water removal at 80 ℃ for 2 h. The nickel promoted catalysts were dried in the presence of air at 110 ℃ and calcined at 550 ℃for 4h [14].

2.4. Characterization

The crystallinity of the samples was determined by X-ray diffraction (Philips, PW1840, CuKα radiation). Field emission-scanning electron microscopy (FE-SEM) images were taken by Mira3-XMU FE-SEM. Surface area, pore size and pore volume were measured

by Brunauer-Emmett-Teller (BET) method using ASAP2420 Micromeritics Adsorption Analyzer. The acidic properties of the samples were determined using temperature-programmed desorption (TPD) of ammonia by AutoChem 2900 (Micromeritics).

2.5. Catalytic evaluation

The catalyst was evaluated in hydrocracking of vacuum gas oil in a stainless-steel fixed bed continuous microreactor loaded with 5 g of the desired catalyst. The vacuum gas oil feedstock properties are shown in Table 1.

The schematic diagram of experimental setup for hydrocracking of vacuum gas oil is shown in Fig. 1. The hydrocracking evaluation was carried out under 400 ℃, a total pressure of 55 bar, a weight hourly space velocity (WHSV) of $1h^{-1}$, and a volumetric hydrogen/oil ratio of 1000 (Nlit/kg). The cylindrical microreactor with 25 cm height and 1.2 cm diameter was equipped with a catalyst bed and a heater whose temperature could be controlled and monitored. Preheated feed that combined by hydrogen gas was pumped into the microreactor and passing through the catalyst bed. After a stabilization period of 5 h, reaction products were collected and analyzed. Catalysts were sulfided in situ at a pressure of 55 bar and 360 ˚C using the mixture of straight run diesel fraction and dimethyl disulfide. The boiling point distribution of liquid products was obtained by simulated distillation method (SIMDIS, ASTM D2887). The liquid products were fractionated into naphtha (90-160 ℃), middle distillate (160-370 $°C$) and the residue product boiling above 370 $°C$. The conversion (Con), selectivity of gas (S_G), selectivity of naphtha (S_N) and selectivity of middle distillates (S_{MD}) were calculated using the equations 1-4.

3. Results and Discussion

The XRD patterns of the zeolites were shown in Fig. 2. These patterns confirmed the preparation of beta zeolite and USY zeolite phase according to JCPDS No. of 47-0183 and 43-0168, respectively.

Crystal diameter of the prepared samples was calculated according to Scherrer equation using the peaks centered at 2θ of 22.5˚ and 6˚ for beta zeolite and USY zeolite, respectively. The obtained crystal diameter of beta zeolite was 16 nm and for USY zeolite was 32 nm.

N_2 adsorption isotherms were used to investigate textural properties of the prepared samples. The BET surface area, pore volume and average pore diameter of the samples were shown in Table 2. It can be concluded from this Table that the value of BET surface area and pore volume in the beta zeolite are higher than those of in USY zeolite

Table1. Vacuum Gas Oil feedstock properties at 20°C and density 0.85 g cm^{-3}.

SIMDIST distillation Fraction (°C)	Values
Gas (<90) %	0
Naphtha (90-160) %	0
Kerosene (160-270) %	0
Gas Oil (270-370) %	5
Vacuum Gas Oil (370-518) %	95

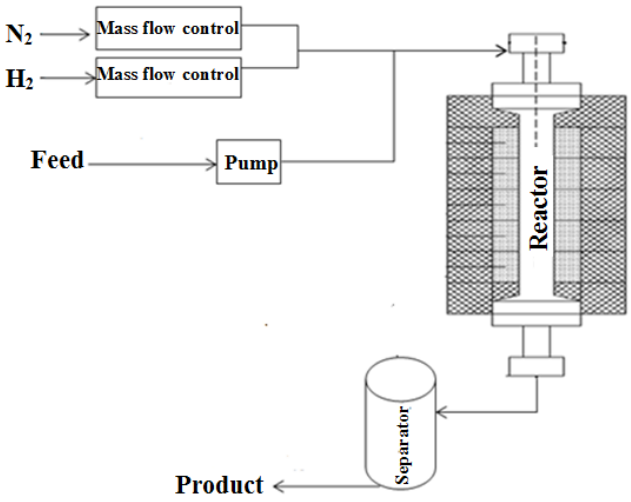

Fig.1. Schematic diagram of experimental setup for the hydrocracking of vacuum gas oil.

$$Con\% = 100\% - \frac{370°C^{+}\ in\ Product(wt\%)}{370°C^{+}\ in\ Feed(wt\%)} \times 100 \quad (1)$$

$$S_G\% = \frac{<90°C\ in\ Product\ (wt\%)}{370°C^{+}\ in\ Feed(wt\%) - 370°C^{+}\ in\ Product(wt\%)} \times 100 \quad (2)$$

$$S_N\% = \frac{(90-160°C) in\ product\ (wt\%)}{370°C^{+}\ in\ Feed(wt\%) - 370°C^{+}\ in\ Product(wt\%)} \times 100 \quad (3)$$

$$S_{MD}\% = \frac{(160-370°C) in\ product\ (wt\%) - (160-370°C) in\ feed\ (wt\%)}{370°C^{+}\ in\ Feed(wt\%) - 370°C^{+}\ in\ Product(wt\%)} \times 100 \quad (4)$$

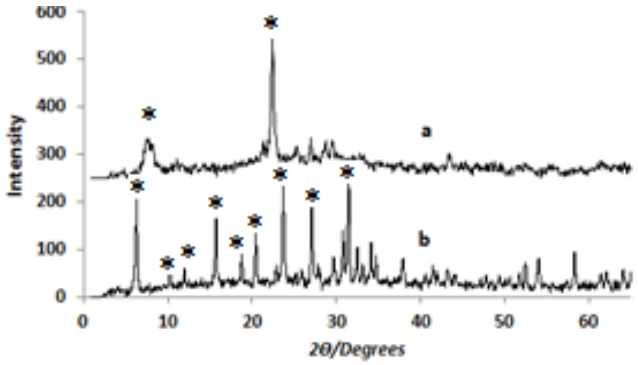

Fig. 2. XRD patterns of (a) beta and (b) USY zeolite (*: Reference peaks).

Also, the support and the catalyst that contains beta zeolite had higher surface area and higher pore volume in comparison to the support and the catalyst containing USY. This could be attributed to the lower crystal diameter of beta zeolite than that of USY zeolite. In addition, the surface area of catalysts decreased due to the addition of metal oxides. It is reasonable because the metal oxides cover a part of surface area of the support. Another point is that the average pore diameter of the support is lower than the corresponding catalyst. This could be attributed to assembling and expanding the metal oxides during the process of calcination of the catalysts, such that some of the catalysts pores, especially micro pores, collapse, resulting in a decrease in the average pore diameter [15].

Nitrogen adsorption-desorption isotherms of the zeolites were shown in Fig. 3a. All of the samples have type IV adsorption/desorption isotherms with a distinct hysteresis loops that confirmed mesoporosity of the samples. Pore size distribution of the samples is shown in Fig. 3b. It confirms that all zeolites have mesoporous structures. Maximum pore diameter of the Ni-Mo/20beta is lower than 10 nm. Thus, this catalyst produces lighter products (naphtha) in hydrocracking process because of diffusion restriction. On the contrary, Ni-Mo/20USY catalyst has uniformly pore size distribution and maximum pore diameter of it is around 50 nm and this results in heavier products (middle distillate) in the hydrocracking process.

Table 2. Physical properties of nanozeolites and the prepared samples.

Samples	Specific surface area (m^2g^{-1})	Pore volume (cm^3g^{-1})	Pore diameter (nm)
ASA	451	1.57	13.7
beta zeolite	639	0.42	2.4
USY zeolite	576	0.36	2.1
20 beta*	326	0.63	7.7
20USY**	310	0.57	8.1
Ni-Mo/20 beta	280	0.54	6.1
Ni-Mo/20USY	247	0.5	7.1

*20 beta: ASA (60%wt.)+ beta nanozeolite (20%wt.)+ binder (20%wt.).
**20USY: ASA (60%wt.)+ USY nanozeolite (20%wt.)+ binder (20%wt.).

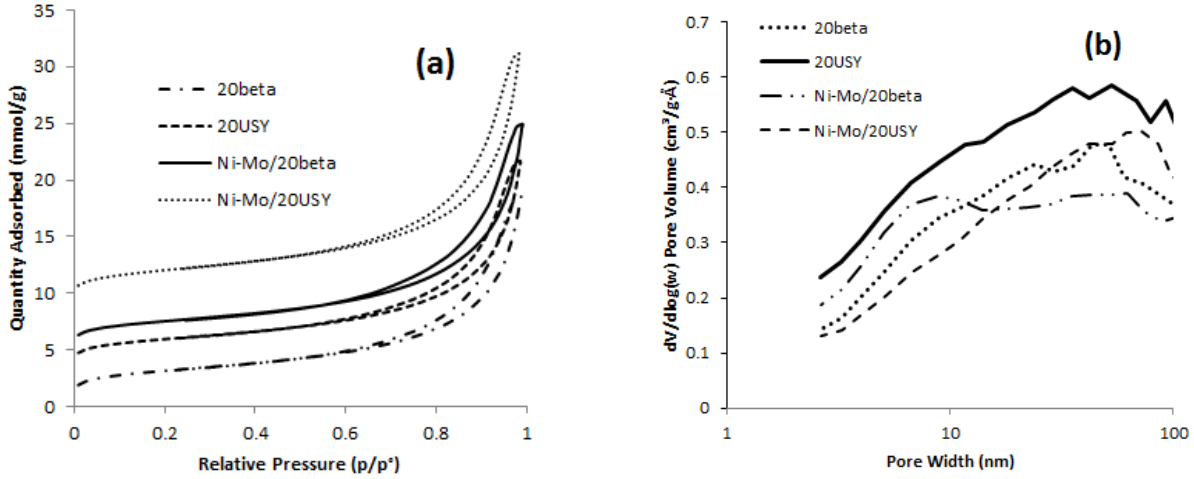

Fig. 3. (a) Nitrogen adsorption-desorption isotherms (b) Pore size distribution of the samples.

The FE-SEM images of the samples were shown in Fig. 3. These images showed the nanoscale size of the zeolites. Average particle size in both zeolites is approximately same. In beta zeolite with the lower crystal diameter, packing of the particle was better than another one.

As can be seen in the Fig. 4, 20USY has more compressive and homogenous than 20 beta. Also, the comparison of the 20 beta and 20USY images shows that lower space among the particles in 20 USY.

The acidities and acid sites distribution on the samples were listed in Table 3. To compare the acidity distribution among the samples, the weak, medium and strong acidities can be seen in Fig. 4. The weak, medium and strong acidities were assigned to the peak areas of NH_3-TPD curves below 350 ℃, at 350-500 ℃, and above 500 ℃, respectively [16]. According to Table 3, the total acidity in 20 USY is higher than 20 beta. In addition, this trend can be seen about the corresponding catalyst. The Si/Al ratio in beta zeolite was higher than USY zeolite and this causes lower weak and total acidity and higher strong acid sites [17].

Weng et al. have shown that the framework silicon could control acidic property and excessive silicon forms silicon islands and decrease total acidity [18]. For both 20beta and 20USY, weak, strong and total acidity were increased after the impregnation of Ni-Mo on them. An incorporation of metals on the composites resulted in enhancement of amounts of acidic sites due to many reasons such as the polarization of metal particles by nearby cations, a direct promotion of positive charge on the metal particles and charge transfer between metal atoms and zeolite oxygen atoms [19].

NH_3-TPD profiles were summarized in Fig. 5. All profiles have two sharp peaks with a temperature around 220 $^{\circ}C$ and 650 $^{\circ}C$. To compare their relative acidity and strength, a Gaussian function was applied to do peak-differentiating and imitating with the two independent peaks recording as weak and strong acidic sites. Also, for all of the samples a shoulder around 450 ℃ was observed that can be attributed to medium acid sites. This shoulder in 20USY and Ni-Mo/20USY is more intensive.

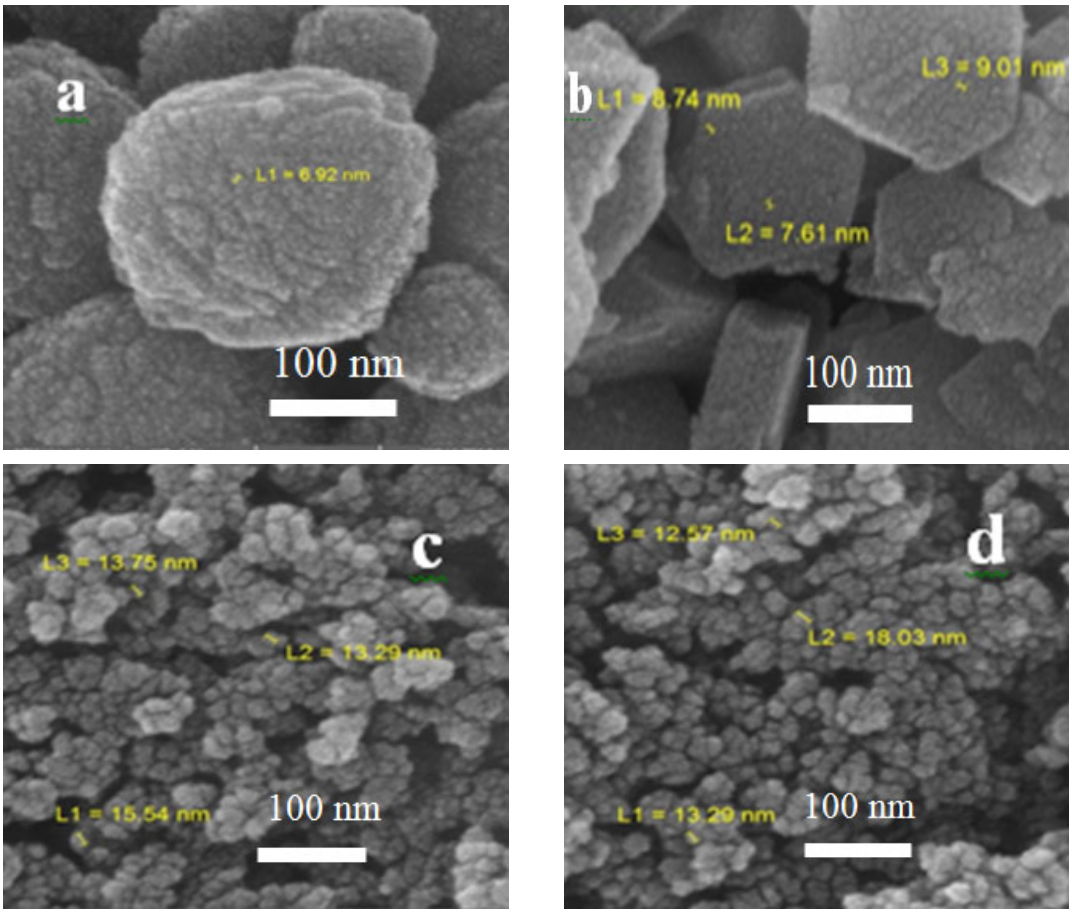

Fig. 4. FE-SEM images of samples (a) beta zeolite, (b) USY zeolite (c), 20 Beta and (d) 20 USY

Table 3. Acidity of the samples.

Samples	Weak acidity (mmol/g)	Strong acidity (mmol/g)	Total acidity (mmol/g)
20 beta	0.8	0.77	1.57
20 USY	1.14	0.63	1.77
Ni-Mo/20 beta	1.34	0.78	2.12
Ni-Mo/20 USY	1.56	0.85	2.41

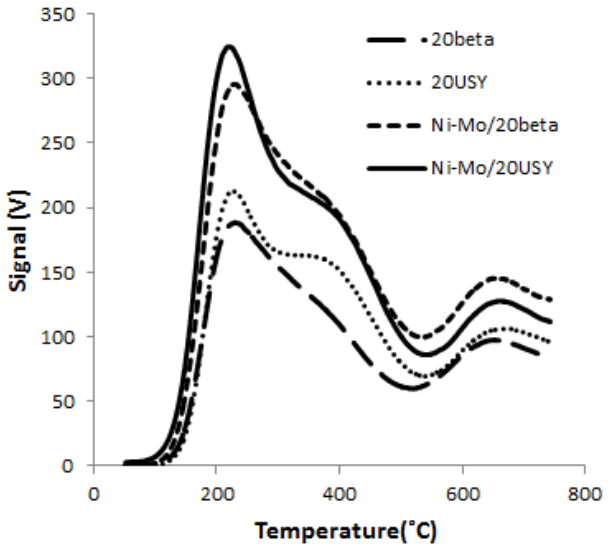

Fig. 5. Ammonia temperature-programmed desorption profiles of the prepared samples.

Table 4 shows the results obtained from hydrocracking of vacuum gas oil in the presence of the prepared catalysts. In addition, the relative results of the commercial catalyst are indicated in this table.

As it is shown in table 4, Ni-Mo/20 USY catalyst has higher selectivity of middle distillate, desirable product, while Ni-Mo/20 beta catalyst has selective in lighter products such as gas and naphtha. Also, it can be concluded that Ni-Mo/20 USY catalyst is more selective in middle distillate than commercial catalysts.

According to Table 3, Ni-Mo/20 USY with higher weak acid sites and Ni-Mo/20 beta with higher strong acid site, cause heavier and lighter products in the hydrocracking process, respectively.

Also, it can be seen in the Table 4 that Ni-Mo/20 beta has higher conversion, that could be attributed to larger surface area of this catalyst.

The significant difference between these two catalysts in hydrocracking may be closely associated with the variations of their acidity properties and the framework structures. The higher acidic density of Ni-Mo/20 USY (2.41 mmol/g) makes the strong acidic sites easily influenced by the reactant molecule adsorption. Therefore, such strong acid strength decreased. Compared with Ni-Mo/20 beta, weaker acidic sites on Ni-Mo/20 USY can participate in the hydrocracking reaction, and then the conversion was reduced.

In addition, the framework structure of beta zeolite makes its pore channels less efficient in diffusing reactant or product molecules than USY zeolite. Beta zeolite has two channels 0.72 nm× 0.62 nm in diameter, and a third channel that is only 0.55 nm× 0.55 nm wide, while USY zeolite has three-dimensional uniform channels with a size about 0.75 nm× 0.75 nm [20]. Thus, the hydrocracking, especially the secondary cracking, occurs in the beta zeolite due to a longer resident time. So, selectivity of lighter products is higher in Ni-Mo/20 beta.

Our results are in accordance with the reports [21] indicating the direct comparison of the catalysts based on Y zeolite and beta zeolite in the hydrocracking of vacuum gas oil, it was found that the catalysts based on beta zeolite had a lower selectivity in middle distillates than the Y zeolite-based catalysts. The catalysts selectivity of gas and naphtha ranged in the reverse sequence compared to the selectivity of middle distillates.

Table 4. Selectivity and conversion of the prepared catalyst in the hydrocracking of vacuum gas oil.

Samples	Selectivity (%)			Conversion (%)
	gas	naphtha	Middle distillate	
Ni-Mo/ 20 beta	22.5	11.3	66.2	44.8
Ni-Mo/ 20 USY	7.1	6.9	87	40.5
Commercial catalyst	5.2	14.3	80.5	41

4. Conclusions

FE-SEM images of prepared USY and beta nanozeolite indicated that the particle size of these zeolites were less than 10 nm. Lower crystal diameter of beta zeolite with respect to that of USY zeolite caused higher pore volume and larger surface area.

USY zeolite with lower Si/Al ratio had more weak and total acidity than beta nanozeolite, while strong acidity of beta nanozeolite was more than USY zeolite. Ni-Mo/20USY catalyst with higher pore diameter and acidity in hydrocracking of vacuum gas oil was more selective compared to middle distillate products, while Ni-Mo/20beta catalyst with higher surface area had higher conversion than others.

References

[1] P.P. Dik, I.G. Danilova, L.S. Golubev, M.O. Kazakov, K.A. Nadeina, S.V. Budukva, V. Yu. Pereyma, O.V. Klimov, I.P. Prosvirin, E. Yu. Gerasimov, T.O. Bok, I.V. Dobrekova, E.E. Knyazeva, I.I. Ivanova, A.S. Noskov, Fuel 237 (2019) 178–190.

[2] Q. Cui, Y. Zhou, Q. Wei, G. Yu, L. Zhu, Fuel Process. Technol. 106 (2013) 439-446.

[3] L-E. Sandoval-Diaz, J-A. Gonzalez-Amaya, C-A. Trujillo, Microporous Mesoporous Mater. 215 (2015) 229-243.

[4] I.C. Neves, G. Botelho, A.V. Machado, P. Rebelo, Eur. Polym. J. 42 (2006) 1541-1547.

[5] Q. Cui, Y. Zhou, Q. Wei, X. Tao, G. Yu, Y. Wang, J. Yang, Energy Fuel 26 (2012) 4664−4670.

[6] J. Francis, E. Guillon, N. Bats, C. Pichon, A. Corma, L.J. Simon, Appl. Catal. A 410 (2011) 140−147.

[7] A.A. Asadi, S.M. Alavi, S.J. Royaee, M. Bazmi, Microporous Mesoporous Mater. 259 (2018) 142-154.

[8] L. Ding, Y. Zheng, Z. Zhang, Z. Ring, J. Chen, J. Catal. 241 (2006) 435-445.

[9] M.A. Ali, T. Tatsumi, T. Masuda, Appl. Catal. A 233 (2002) 77–90.

[10] D. Karami, N. Mahinpey, Chem. Engin. Commun. 203 (2016) 251-257.

[11] L. Ding, Y. Zheng, H. Yang, R. Parviz, App. Catal. A 353 (2009) 17–23.

[12] M. Heuchel, Ch. Dörr, R. Boldushevskii, S. Lang, E. Klemm, Y. Traa, Appl. Catal. A 553 (2018) 91–106.

[13] S. Chen, T. Li, G. Cao, M. Guan, US Pat. (2002) 6 399 530.

[14] C. Leyva, M.S. Rana, F. Trejo, J. Ancheyta. Catal. Today. 141 (2009) 168–175.

[15] M. Majka, G. Tomaszewicz, A. Mianowski, J. Energy Instit. 91 (2018) 1164-1176.

[16] J. Jiang, Zh. Dong, H. Chen, J. Sun, Ch. Yang, F. Cao, Energy Fuel 27 (2013) 1035-1039.

[17] M. Subsadsana, P. Kham-or, P. Sangdara, P. Suwannasom, Ch. Ruangviriyachai, J. Fuel. Chem. Technol. 45 (2017) 805-816.

[18] X. Wang, F. Guo, X. Wei, Z. Liu, W. Zhang, S. Guo, L. Zhao, Korean J. Chem. Eng. 33 (2016) 2034–2041.

[19] C. Manrique, A. Guzmán, J. Pérez-Pariente, C. Márquez-Álvarez, A. Echavarría, Microporous Mesoporous Mater. 234 (2016) 347-360.

[20] L. Ding, Y. Zheng, Z. Zhang, Z. Ring, J. Chen, Appl. Catal. A 319 (2007) 25–37.

[21] A. Hassan, S. Ahmed, M.A. Ali, H. Hamid, T. Inui, Appl. Catal. A 220 (2001) 59–68.